FULL PAPER

Self-Powered Trajectory, Velocity, and Acceleration Tracking of a Moving Object/Body using a Triboelectric Sensor

Fang Yi, Long Lin, Simiao Niu, Jin Yang, Wenzhuo Wu, Sihong Wang, Qingliang Liao, Yue Zhang, and Zhong Lin Wang**

Motion tracking is of great importance in a wide range of fields such as automation, robotics, security, sports and entertainment. Here, a self-powered, single-electrode-based triboelectric sensor (TES) is reported to accurately detect the movement of a moving object/body in two dimensions. Based on the coupling of triboelectric effect and electrostatic induction, the movement of an object on the top surface of a polytetrafluoroethylene (PTFE) layer induces changes in the electrical potential of the patterned aluminum electrodes underneath. From the measurements of the output performance (open-circuit voltage and short-circuit current), the motion information about the object, such as trajectory, velocity, and acceleration is derived in conformity with the preset values. Moreover, the TES can detect motions of more than one objects moving at the same time. In addition, applications of the TES are demonstrated by using LED illuminations as real-time indicators to visualize the movement of a sliding object and the walking steps of a person.

1. Introduction

Motion monitoring is increasingly needed for various applications such as automatic control, robotics, and surveillance.[1–3] Traditional motion sensors, which usually rely on optical, microwave, or acoustic sound, have greatly promoted the development of motion sensing technologies.[4–6] These sensors always face a trade-off between the quality of detection and the simplicity in signal processing.[1–7] Most importantly, most of these sensors are not able to work without an external power source. To address this issue, the concept of self-powered/active sensor was introduced,[8] which employs the electrical output of a nanogenerator while triggered by mechanical stimuli. The sensor itself does not need an external power at least and the whole sensor system can be self-powered if enough energy can be acquired from the environment. Recently, triboelectric nanogenerators (TENGs) have been invented for mechanical energy harvesting based on the coupling of the triboelectric effect and electrostatic induction.[9–18] Furthermore, self-powered/active sensors on the basis of the TENGs were developed for various applications such as pressure mapping, ultraviolet detection, and chemical sensing.[19–25] Efforts have also been devoted to utilize the TENGs for self-powered motion tracking in one dimension.[26–28]

In this work, we report a new type of self-powered triboelectric sensor (TES) structured with grounded electrodes to monitor two-dimensional movements. Owing to the triboelectric effect and electrostatic induction, when a charged object moves on the top surface of a thin layer of polytetrafluoroethylene (PTFE), the electric potential of the thin aluminum (Al) electrode underneath the PTFE layer changes over time, thus, charge transfer occurs between the Al electrode and the ground in order to balance the electrostatic potential. The trajectory, velocity, and acceleration of the moving object were detected through the measured open-circuit voltage and short-circuit current in real time. The velocity of the object in uniform motion can also be detected by utilizing the amplitude of the short-circuit current, and a sensitivity of $\approx$887 pA/(cm s^{-1}) was demonstrated. Additionally, LED illuminations were used as real-time indicators for direct visualization of the motion of a sliding object and the walking steps of a person. This research has potential applications in health monitoring, transportation control, sports, entertainment and security system.

F. Yi, L. Lin, S. Niu, Dr. J. Yang, Dr. W. Wu,
Dr. S. Wang, Prof. Z. L. Wang
School of Materials Science and Engineering
Georgia Institute of Technology
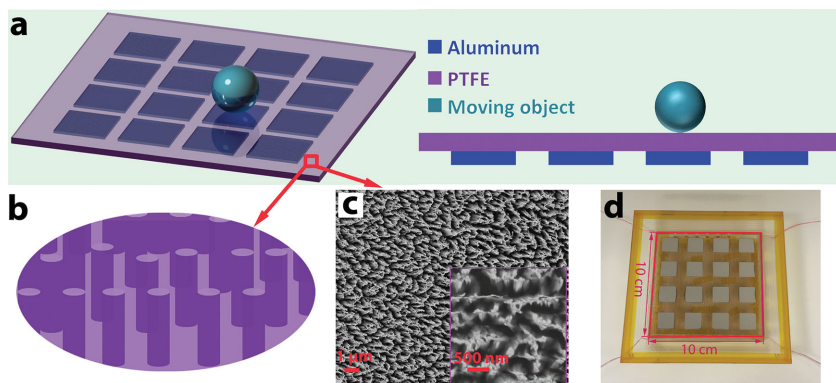Atlanta, Georgia 30332–0245, USA
E-mail: zlwang@gatech.edu

F. Yi, Dr. Q. Liao, Prof. Y. Zhang
State Key Laboratory for Advanced Metals and Materials
School of Materials Science and Engineering
University of Science and Technology Beijing
Beijing 100083, China
E-mail: yuezhang@ustb.edu.cn

F. Yi, Dr. Q. Liao, Prof. Y. Zhang
Key Laboratory of New Energy Materials and Technologies
University of Science and Technology Beijing
Beijing 100083, China

Prof. Z. L. Wang
Beijing Institute of Nanoenergy and Nanosystems
Chinese Academy of Sciences
Beijing 100083, China

2. Results and Discussion

As shown in **Figure 1**a, a TES is composed of two components, with a 50 µm-thick layer of PTFE at the top and patterns of 200 nm-thick Al films at the bottom. The upper surface of the
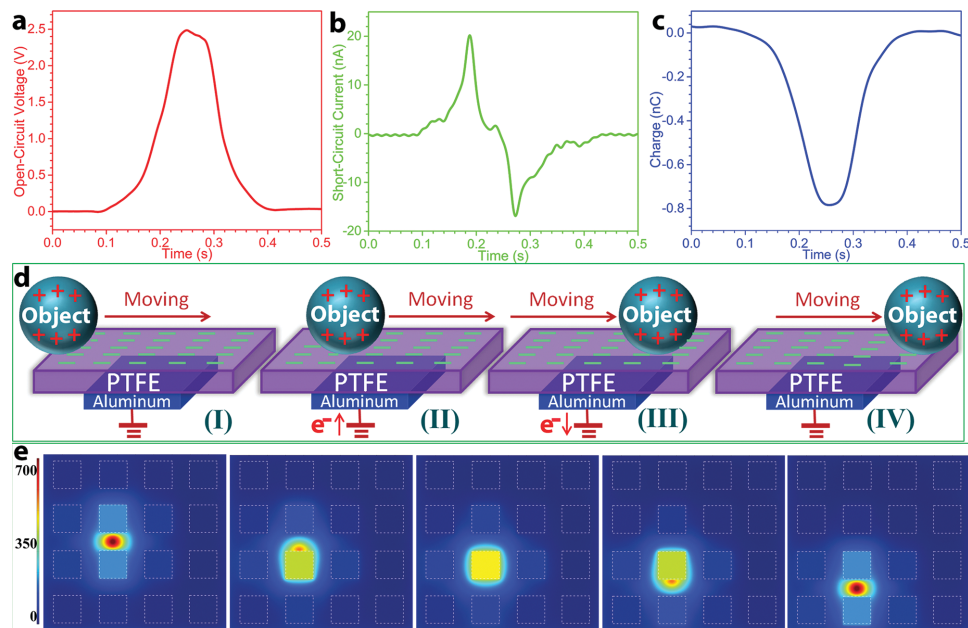
FULL PAPER

Figure 1. Structure of a TES. a) Schematic diagram of the TES and its cross-section view. b) Magnified schematic of the etched PTFE surface. c) FESEM image of the nanorod-structured PTFE surface. The inset shows a view at a higher magnification. d) Optical photograph of the TES, with each electrode having a size of 1.5 cm × 1.5 cm.

PTFE was dry-etched to produce aligned nanorod structures (Figure 1b,c), which could increase the effective surface area and thus improve the triboelectric charge density on the surface.[29,30] A photograph of an as-fabricated TES is presented in Figure 1d, which has a device area of 10 cm × 10 cm. Each square Al electrode in the 4×4 matrix pattern has a side length of 1.5 cm, and the gap between two adjacent Al electrodes is 1 cm. The detailed fabrication process is described in the Experimental Section.

Figure 2a–c display the electrical characteristics of an Al electrode when an Al ball with a diameter of 1.27 cm moves across the PTFE thin film above the electrode (the Al ball involved in the following paragraphs has the same diameter of 1.27 cm

unless otherwise indicated), from which the open-circuit voltage, the short-circuit current and the corresponding charge transfer were recorded. The working principle is schematically depicted in Figure 2d. Since the surface of PTFE has a much stronger ability to attract electrons, it will get negatively charged while there will be net positive charges on the surface of the Al ball after the Al ball rolls over on the PTFE. The generated negative charges on the PTFE surface will be preserved for an extended period of time.[31] When the positively charged ball moves towards an Al electrode lying beneath the PTFE, the potential of the Al electrode will be raised up in the open-circuit condition, and electrons will be driven to flow from the ground to this Al electrode in the short-circuit condition. The amount of the transferred charges and the electric potential both reach their maximum values when the ball arrives at the point over the center of the Al electrode. Then as the ball travels away, the electrical potential of the Al electrode will decline until it reaches its initial state, and electrons will flow back to the ground. Figure 2e illustrates the numerical calculations showing the evolution of electrical potential distribution in the open-circuit condition when the Al ball moves across an arbitrary electrode. In the established model, the thickness of the PTFE and the Al film were assigned to be 500 μm and 100 μm, respectively; and the triboelectric charge density on the top surface of the PTFE was set to be 0.1 μC m^{-2}. A reference electrode was set under the Al film as the ground. It should be mentioned that the alteration of these parameters
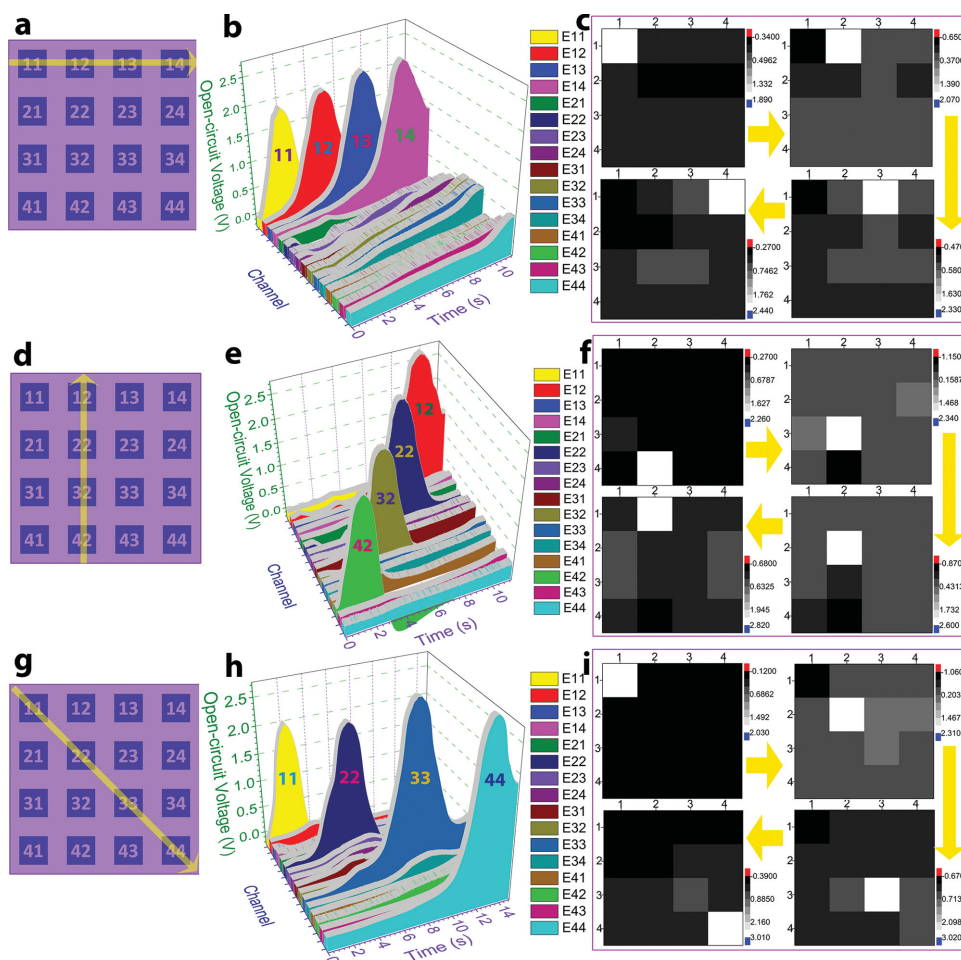

Figure 2. Electrical signals from one electrode, working principle and COMSOL calculation results of the TES. a–c) Electrical measurements of an Al ball moving across a paricular electrode of the TES: a) open-circuit voltage, b) short-circuit current, c) output charges. d) Working mechanism of the TES. e) Finite-element simulation of the potential distribution on the TES when a moving ball is far from, reaches the edge of, arrives at the center of, leaves the edge of, is far away from the electrode underneath the PTFE layer.
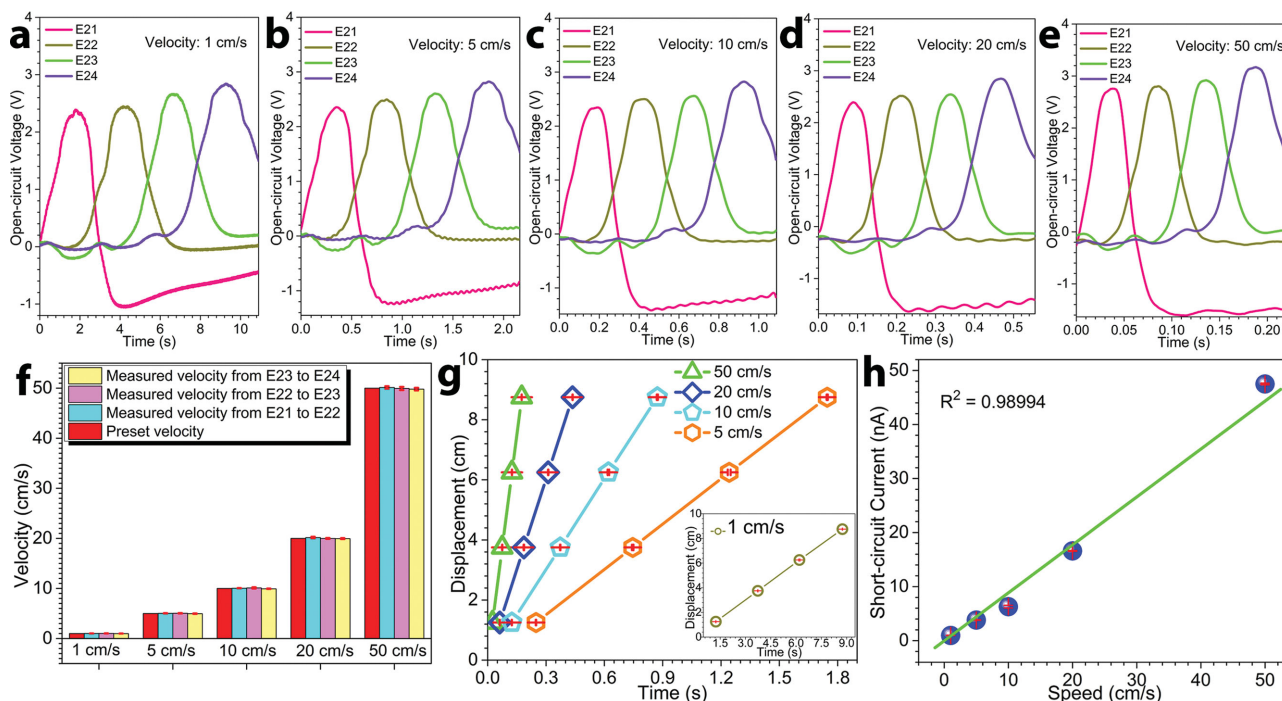
only influences the magnitude of the calculated electrical potential, and the relative changing trend of the electrical potential will be retained. Hence the calculated output characteristics will accurately reflect the working behavior of the TES. From the calculated results in Figure 2e, it can be found that electrodes closer to the positively charged Al ball have larger electrical potential; moreover, the potential level of an electrode increases as its distance to the Al ball reduces. These calculation results are in consistent with the measured output characteristics and thus confirm the validity of the proposed working principle of the TES. It is worth noting that the material of the moving object can be replaced by other kinds of materials such as Nylon, paper, PET, etc. Since PTFE is one of the best materials for creating tribocharger, it always tends to become negatively charged after coming into contact with other materials ranking higher than PTFE in the triboelectric series. And the further away the other material is from PTFE, the greater the charge transferred between the two materials. Using a material different from PTFE of the moving object will only affect the magnitude of the measured electrical signal, but will not impact the

relative changing trend of the electrical signal or the working principle of the sensor.

In order to quantitatively characterize the TES's response to a motion, the Al ball was attached to a linear motor, and the sensor was fixed under the ball to detect its movement. A multichannel measurement system was utilized to record the output signals from each electrode separately. Details on the measurement setup can be found in the Experimental Section and Supporting Information Figure S1. As exhibited in **Figure 3**, when the Al ball moves on the TES along the path: electrode 11 (E11) → electrode 12 (E12) → electrode 13 (E13) → electrode 14 (E14) (Figure 3a), the open-circuit voltage of the electrode that the ball passes through rises to a peak and then decreases (Figure 3b). As discussed earlier, the peak value of the output voltage from a certain electrode occurs when the ball arrives at the point over the center of the electrode. In this regard, a two-dimensional contour plot of the values of output voltage from all electrodes is obtained when the ball gets to the center of an electrode, which explicitly indicates the moving path of the ball (Figure 3c). In a similar way, when the ball moves along the

Figure 3. Motion imaging of an Al ball moving on the TES. a,d,g) Illustration of the ball moving along a path a) from E11 to E14, d) from E42 to E12, g) from E11 to E44. b,e,h) Measured open-circuit voltage of the TES when the ball moves from b) E11 to E14, e) E42 to E12, h) E11 to E44. c,f,i) Mapping figures obtained from the values of open-circuit voltage when the ball gets to the point over the center of an electrode: c) E11→E12→E13→E14, f) E42→E32→E22→E12, i) E11→E12→E13→E14. Note: the Al ball moves at a preset speed of 20 cm s^{-1}.

Figure 4. Detection of velocity and displacement. a–e) Measured open-circuit voltage as an Al ball moves across a path (E21→E22→E23→E24) at a preset speed of a) 1 cm s⁻¹, b) 5 cm s⁻¹, c) 10 cm s⁻¹, d) 20 cm s⁻¹, e) 50 cm s⁻¹. f) Detected velocity of the ball by the TES and the preset velocity of the ball. g) Detected displacement of the ball over time. h) Plot of short-circuit current as a function of speed.

path: E42 → E32 → E22 → E12 (Figure 3d) and E11 → E22 → E33 → E44 (Figure 3g), the recorded out-put voltage of the sensor (Figure 3e,h) can clearly demonstrate the movement of the ball, and the mapping figures plotted at the moment when the ball arrives at the center of a particular electrode intuitively display the path that the ball passes through (Figure 3f,i).

Since the interval between the centers of two neighboring electrodes is a constant that was determined when constructing the sensor, we can not only recognize when a moving object reaches which electrode but also acquire other information, such as the displacement, velocity, and acceleration of the object. **Figure 4**a–e shows the measured results of the open-circuit voltage when the Al ball moves on the sensor with different velocities. Since there are hardly any responses from the electrodes out of the corresponding moving path (Figure 3), signals of those electrodes were omitted from the graphs for simplicity. It should be noted that the same treatments were made to graphs discussed in the following paragraphs. By simply dividing the distance between two electrodes by the time taken to cover the distance, the velocity from one electrode to another can be derived. As presented in Figure 4f, the detected velocity and the preset velocity of the ball between two electrodes have a very good match, with an average error of ≈0.265%. With the known location of each electrode on the sensor, the displacement of the moving ball over time can be easily derived, which is presented in Figure 4g. Note that the origin of the displacement is at the edge of the device area. As the zero-crossing of the short-circuit current is the instantaneous time at which the ball reaches the point over the center of the electrode, the velocity and displacement of the moving ball can also be detected by measuring the short-circuit current in a way similar

to using the open-circuit voltage (Figure S2, Supporting Information). Moreover, the velocity of the ball in uniform motion can be detected by analyzing the amplitude of the short-circuit current. The short-circuit current of the TES can be given as:

$$I_{sc} = dQ_{sc}/dt = (dQ_{sc}/dx)(dx/dt) = (dQ_{sc}/dx)v \tag{1}$$
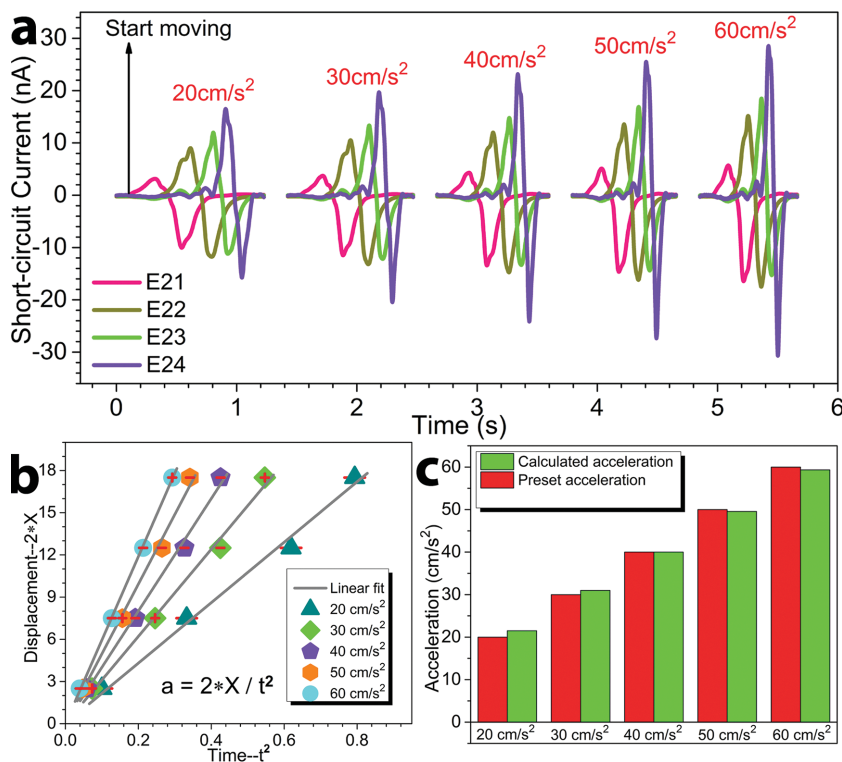
where Q_{sc} is the short-circuit transferred charges, x is the distance between the object and the electrode, and v is the velocity of the object. For uniform motion, the amplitude of the short-circuit current can be given as:[32]

$$I_{sc\text{-}peak} = (dQ_{sc}/dx)_{peak} v \tag{2}$$

which means that the amplitude of the short-circuit current is linearly dependent on the velocity. The measured relationship between the amplitude of the short-circuit current and the velocity of the ball is exhibited in Figure 4h, from which a sensitivity of ≈887 pA/(cm s⁻¹) can be achieved with good linearity ($R^2 ≈ 0.99$). This can be applied to detect the velocity of an object when recording time is not available, provided that the space charge distribution is the same. The value of the short-circuit current at a certain speed in Figure 4h is the average peak value of short-circuit current from all the electrodes that the ball passes through during the travel.

Figure 5 exhibits the ability of the sensor to detect non-uniform motion of a moving object. Shown in Figure 5a is the short-circuit current measured as the Al ball moves on the sensor with different accelerations. Under a certain acceleration, the amplitudes of the short-circuit current from the electrodes increase in a timed sequence as the ball passes across

Figure 5. Acceleration detection by analyzing the short-circuit current. a) Measured short-circuit current when an Al ball passes across a path (E21→E22→E23→E24) with different accelerations. b) Twice the displacement versus square of time. The slope of the fitted line is the acceleration detected by the TES. c) Detected acceleration and the preset acceleration of the moving ball.

these electrodes. Also, the amplitude of the short-circuit current from each electrode becomes higher with the increasing acceleration of the ball. As the ball starts from rest at the edge of the device area and accelerates uniformly, the acceleration of the ball moving across the sensor can be computed by using the formula:

$$a = 2x/t^2 \qquad (3)$$

where t is the time taken to travel from the origin point to a particular electrode, x is the displacement over the time interval, and a is the acceleration during the travel. Figure 5b is plotted according to Equation 3, in which the correlation between $2x$ and t^2 was linearly fitted, and the slopes of the fitted curves are the accelerations detected by the TES. As shown in Figure 5c, the detected accelerations are in good agreement with the preset ones, with an average error of ≈2.5%.

The TES is also capable of detecting motion of more than one object moving simultaneously. From the open-circuit voltage in response to the motion of two balls in Figure S3a (Supporting Information), the information about the position, velocity, and displacement for both of the two balls can be acquired. The velocities of the two balls can be calculated using the aforementioned method, which is shown in Figure S3b. Figure S3c presents the detected position and displacement of the two balls, in which the origin of the displacement is at the edge of the device area. The space between the two balls can

also be estimated by multiplying the velocity by the time interval, which is approximately 3.99 cm.

To achieve a comprehensive understanding about the performance of the triboelectric motion sensor, the influences of several important parameters (size of electrodes, number of electrodes, and size of the moving object) on the performance of the TES have been systematically investigated, and the results are shown in Supporting Information Figure S4–S7. First, if the number of electrodes remains unchanged in a fixed device area, enlarging the size of each electrode will enhance the open-circuit voltage, but will not affect the peak position of the open-circuit voltage in the time scale (Figure S4d). The increase in the open-circuit voltage for larger electrodes can be associated with the increased amount of transferred charges between the electrode and the ground (Figure S4e). Second, the number of electrodes on the sensor will have a major impact on the characteristics of the sensor. As shown in Figure S5, when the Al ball moves along a certain path on sensors with different numbers of Al electrodes (Figure S5a–c), more existing electrodes result in more peaks of open-circuit voltage within the same displacement (Figure S5d–g) and thus more precise motion information for the moving object. Since the electrodes divide the device area into equal parts and a peak value of open-circuit voltage appears as an object gets to the center of each part, increasing the number of electrodes in a fixed device area can be thought of as improving the spatial resolution of the triboelectric motion sensor. If there is a fixed area ratio of the electrode to the part it stays in, raising the number of electrodes in a fixed device area means decreasing the size of each electrode. As discussed above, reducing the size of the electrode will lower the open-circuit voltage; thereby there should be a maximum number of electrodes within a device area that can clearly identify each peak of the open-circuit voltage, which can be calculated through a numerical method.[32,33] In the calculation model, a TES with a device area of 2 cm × 2 cm was selected. The diameter of the moving Al ball was set to be 1.27 cm, and the ratio between the side length of each square electrode (SL-electrode) and the side length of each part that an electrode stays in (SL-part) was set to be 3/5. From the calculated results shown in Figure S6, it can be found that there is a huge drop in the ratio of the open-circuit voltage from one electrode (V_{oc}) to the open-circuit voltage from the electrode next to this electrode ($V_{oc\text{-}adjacent}$) when the side length of each part is below 3.33 mm. If the minimum $V_{oc}/V_{oc\text{-}adjacent}$ ratio is set to be 1.1 so as to distinguish peak values of the measured open-circuit voltage, the maximum number of electrodes on this TES will be 1600, which equals to 4 electrodes per square millimeter. The numerical simulation of the electrical potential distribution on the TES with the maximum electrode density is illustrated in

Figure S6b,c. It should be mentioned that changing the ratio of SL-electrode/SL-part or the ratio of $V_{oc}/V_{oc\text{-adjacent}}$ will result in a different maximum number of electrodes, and the maximum number of electrodes in a fixed device area should be adjusted according to actual conditions. This result demonstrates the possibilities as well as the limitations to further develop the performance of the triboelectric motion sensor for high spatial resolution. Third, for a sensor with a fixed device area and fixed number/size of electrodes, a bigger moving object will lead to higher open-circuit voltage (Figure S7a) and induce a larger quantity of transferred charges between the electrode and the ground (Figure S7b). From Figure S7a it can also be observed that the size of the moving object has no influence on the peak position of the open-circuit voltage of the sensor.
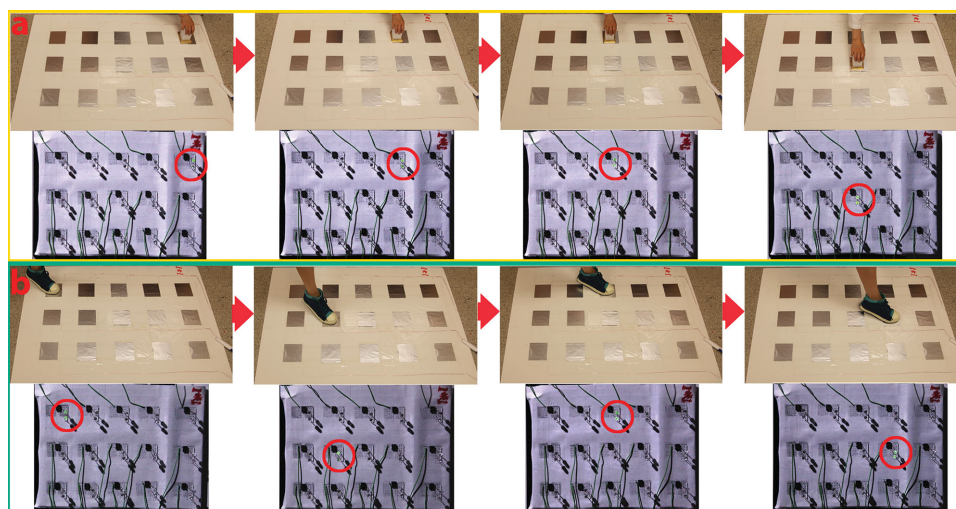
The concept of the fabricated triboelectric motion sensor can be applied for widespread domestic and commercial applications, such as monitoring the movement of people in a building, security control, automatic control, and so on. Compared with traditional motion sensors that rely on optical signal, microwave, or acoustic sound, our TES has great advantages in terms of low cost, no external power consumption, real-time recording and simple signal processing. Figure S8 (Supporting Information) exhibits the open-circuit voltage response of the TES when the Al ball moves a distance of 1 mm on the sensor, which presents a high sensitivity of 0.45 V mm^{-1} and good repeatability. As exhibited in Figure S8b, the TES shows a fast response time of ≈16.5 ms, which is the time required to output a signal for the movement of the ball. The response time of a circuit mainly depends on the Resistive-Capacitive (RC) delay, which occurs when a step voltage or signal is firstly applied to the circuit. For an actual circuit, the RC time constant cannot be ignored, and it is decided by the RC effects of all the nodes in the whole circuit, including the TES and the circuit of the measuring instrument. The reliability and stability of the sensor was investigated through reciprocating movement of the Al ball on the sensor. As shown in Figure S9, there is no significant change in the magnitude of the measured electrical signals

and nearly no change in the peak position of the open-circuit voltage after about 3000 cycles of periodic motion, indicating high reliability and stability in device operation.

In **Figure 6**, two simplified applications of the self-powered triboelectric motion sensor are demonstrated by using LED illuminations as the motion indicator. A TES having an area of 112 cm × 77 cm was constructed with Al electrodes uniformly distributed in a 5 × 3 matrix under a 50 μm-thick PTFE film. Each square Al electrode had a side length of 10 cm, and the space between two neighboring electrodes was also 10 cm. There was a bundle of LED lights connected to each Al electrode, which formed a 5 × 3 matrix the same as the Al electrodes. When an Al plate slides through a certain electrode on the sensor, the bundle of LEDs corresponding to this electrode would be lighted up (Figure 6a and Video S1, Supporting Information). Furthermore, the TES can be used to detect the walking steps of a person. As shown in Figure 6b and Video S2 (Supporting Information), when a human walks on the TES, every step of the person can be located through the bundle of lighted LEDs that are connected to the electrode the person steps on.

3. Conclusion

In summary, we developed a novel type of self-powered, single-electrode-based motion sensor on the basis of the triboelectric effect. The trajectory, velocity, and acceleration of moving objects were accurately detected through real-time recording of the open-circuit voltage and short-circuit current from the TES. Systematic investigations were carried out to study the influence of various factors on the sensor performance and elucidate its future optimization. LED illuminations were used to visualize the applications of the TES, which were lighted up by the TES and served as indicators to monitor the motion of a sliding object and the walking steps of a person in real time. This triboelectric motion sensor has significant advantages

Figure 6. Demonstration of the self-powred TES for motion monitoring. a) Top: photographs of an object sliding on a TES with the same working principle as the previously expounded one. Bottom: photographs of LED bundles lighted up by the TES. There is a one-to-one relationship between bundles of LEDs and electrodes of the TES. b) Top: photographs of human foot walking on the TES. Bottom: photographs of LED bundles lighted up by the TES.

www.MaterialsViews.com

ADVANCED
FUNCTIONAL
MATERIALS
www.afm-journal.de

FULL PAPER

such as no external power supplies, low cost, real-time monitoring, simple signal processing, and high reliability. This work opens up new possibilities for self-powered motion detection and new perspectives for the practical applications of the TENGs.

4. Experimental Section

Fabrication of a TES: 1. A 50-μm thick PTFE film was dry-etched to create the nanorod structures by applying the inductively coupled plasma (ICP) method: the etching time was 40s; and the flow rate of Ar, O_2, and CF_4 gases were 15.0 sccm, 10.0 sccm, and 30.0 sccm, respectively. 2. A PET mask with a hollow matrix pattern was made by laser-cutting. 3. Al film with a thickness of 200 nm was deposited on the non-etched side of PTFE through windows of the PET mask by sputtering. 4. The Al film was connected to metal wires by using the silver paste.

Morphology Characterization of the TES: The morphology of the etched PTFE surface was characterized by a field emission scanning electron microscope (Hitachi SU8010).

Operation setup for the TES: 1. Fix the TES onto an acrylic plate and put it under a linear motor. 2. Put an Al ball inside a short acrylic tube having a diameter slightly bigger than the ball. 3. Mount the acrylic tube on the linear motor, and adjust the distance between the tube and the TES underneath so that the ball can roll on the TES. 4. The metal wire from each Al electrode is connected to a separate channel of the multichannel measurement system, and the other end of each channel is connected to the ground.

Supporting Information

Supporting Information is available from the Wiley Online Library or from the author.

Acknowledgements

[1] S. Etaki, M. Poot, I. Mahboob, K. Onomitsu, H. Yamaguchi, H. S. J. van der Zant, *Nat. Phys.* **2008**, *4*, 785–788.

[2] J. Hightower, G. Borriello, *Computer* **2001**, *34*, 57–66.

[3] T. Yamada, Y. Hayamizu, Y. Yamamoto, Y. Yomogida, A. Izadi-Najafabadi, D. N. Futaba, K. Hata, *Nat. Nanotechnol.* **2011**, *6*, 296–301.

[4] T. W. Kenny, S. B. Waltman, J. K. Reynolds, W. J. Kaiser, *Appl. Phys. Lett.* **1991**, *58*, 100–102.

[5] J. C. Lin, *Bioelectromagnetics* **1992**, *13*, 557–565.

[6] R. E. Rinehart, E. T. Garvey, *Nature* **1978**, *273*, 287–289.

[7] A. Borst, M. Egelhaaf, *Trends Neurosci.* **1989**, *12*, 297–306.

[8] Z. L. Wang, *Adv. Mater.* **2012**, *24*, 280–285.

[9] C. Bao Han, W. Du, C. Zhang, W. Tang, L. Zhang, Z. Lin Wang, *Nano Energy* **2014**, *6*, 59–65.

[10] F.-R. Fan, Z.-Q. Tian, Z. Lin Wang, *Nano Energy* **2012**, *1*, 328–334.

[11] S. Lee, Y. Lee, D. Kim, Y. Yang, L. Lin, Z.-H. Lin, W. Hwang, Z. L. Wang, *Nano Energy* **2013**, *2*, 1113–1120.

[12] S. Wang, L. Lin, Z. L. Wang, *Nano Lett.* **2012**, *12*, 6339–6346.

[13] S. Wang, L. Lin, Y. Xie, Q. Jing, S. Niu, Z. L. Wang, *Nano Lett.* **2013**, *13*, 2226–2233.

[14] S. Wang, Y. Xie, S. Niu, L. Lin, Z. L. Wang, *Adv. Mater.* **2014**, *26*, 2818–2824.

[15] Y. Xie, S. Wang, S. Niu, L. Lin, Q. Jing, Y. Su, Z. Wu, Z. L. Wang, *Nano Energy* **2014**, *6*, 129–136.

[16] Y. Yang, G. Zhu, H. Zhang, J. Chen, X. Zhong, Z.-H. Lin, Y. Su, P. Bai, X. Wen, Z. L. Wang, *ACS Nano* **2013**, *7*, 9461–9468.

[17] G. Zhu, J. Chen, T. Zhang, Q. Jing, Z. L. Wang, *Nat. Commun.* **2014**, *5*, 3426.

[18] G. Zhu, Z.-H. Lin, Q. Jing, P. Bai, C. Pan, Y. Yang, Y. Zhou, Z. L. Wang, *Nano Lett.* **2013**, *13*, 847–853.

[19] Y. Hu, J. Yang, Q. Jing, S. Niu, W. Wu, Z. L. Wang, *ACS Nano* **2013**, *7*, 10424–10432.

[20] L. Lin, Y. Xie, S. Wang, W. Wu, S. Niu, X. Wen, Z. L. Wang, *ACS Nano* **2013**, *7*, 8266–8274.

[21] Z.-H. Lin, G. Cheng, W. Wu, K. C. Pradel, Z. L. Wang, *ACS Nano* **2014**, *8*, 6440–6448.

[22] Z.-H. Lin, G. Cheng, Y. Yang, Y. S. Zhou, S. Lee, Z. L. Wang, *Adv. Funct. Mater.* **2014**, *24*, 2810–2816.

[23] Y. Yang, H. Zhang, Z.-H. Lin, Y. S. Zhou, Q. Jing, Y. Su, J. Yang, J. Chen, C. Hu, Z. L. Wang, *ACS Nano* **2013**, *7*, 9213–9222.

[24] H. Zhang, Y. Yang, Y. Su, J. Chen, K. Adams, S. Lee, C. Hu, Z. L. Wang, *Adv. Funct. Mater.* **2014**, *24*, 1401–1407.

[25] H. Zhang, Y. Yang, Y. Su, J. Chen, C. Hu, Z. Wu, Y. Liu, C. Ping Wong, Y. Bando, Z. L. Wang, *Nano Energy* **2013**, *2*, 693–701.

[26] Y. Su, G. Zhu, W. Yang, J. Yang, J. Chen, Q. Jing, Z. Wu, Y. Jiang, Z. L. Wang, *ACS Nano* **2014**, *8*, 3843–3850.

[27] Y. Yang, H. Zhang, J. Chen, Q. Jing, Y. S. Zhou, X. Wen, Z. L. Wang, *ACS Nano* **2013**, *7*, 7342–7351.

[28] Y. S. Zhou, G. Zhu, S. Niu, Y. Liu, P. Bai, Q. Jing, Z. L. Wang, *Adv. Mater.* **2014**, *26*, 1719–1724.

[29] H. Fang, W. Wu, J. Song, Z. L. Wang, *J. Phys. Chem. C* **2009**, *113*, 16571–16574.

[30] G. Zhu, C. Pan, W. Guo, C.-Y. Chen, Y. Zhou, R. Yu, Z. L. Wang, *Nano Lett.* **2012**, *12*, 4960–4965.

[31] F. Saurenbach, D. Wollmann, B. D. Terris, A. F. Diaz, *Langmuir* **1992**, *8*, 1199–1203.

[32] S. Niu, Y. Liu, S. Wang, L. Lin, Y. S. Zhou, Y. Hu, Z. L. Wang, *Adv. Funct. Mater.* **2014**, *24*, 3332–3340.

[33] S. Niu, S. Wang, Y. Liu, Y. S. Zhou, L. Lin, Y. Hu, K. C. Pradel, Z. L. Wang, *Energy Environ. Sci.* **2014**, *7*, 2339–2349.